Atom Interferometry with the Sr Optical Clock Transition

Liang Hu,* Nicola Poli,† Leonardo Salvi, and Guglielmo M. Tino‡
Dipartimento di Fisica e Astronomia and LENS - Università di Firenze, INFN - Sezione di Firenze, Via Sansone 1, I-50019 Sesto Fiorentino, Italy
(Received 15 August 2017; published 27 December 2017)

We report on the realization of a matter-wave interferometer based on single-photon interaction on the ultranarrow optical clock transition of strontium atoms. We experimentally demonstrate its operation as a gravimeter and as a gravity gradiometer. No reduction of interferometric contrast was observed for a total interferometer time up to ∼10 ms, limited by geometric constraints of the apparatus. Single-photon interferometers represent a new class of high-precision sensors that could be used for the detection of gravitational waves in so far unexplored frequency ranges and to enlighten the boundary between quantum mechanics and general relativity.

DOI: 10.1103/PhysRevLett.119.263601

Matter-wave interference enables the investigation of physical interactions at their fundamental quantum level and forms the basis of high-precision inertial sensors and for application in precision gravitational field sensing [1]. Today's best atom interferometers (AIs), based on multiphoton Raman or Bragg transitions and Bloch oscillations, can tailor matter waves at will, up to macroscopic scales [2], preserving their coherence for extremely long times [3], allowing precision measurements of the Newtonian gravitational constant [4], Earth gravity acceleration [5–7], gravity gradients [8,9], and gravity curvature [10,11]. At the same time, optical spectroscopy of ultranarrow optical transitions in atoms and ions has produced clocks with the highest relative frequency accuracy, approaching the 10^{-19} level [12–15]. Thanks to these impressive results, schemes for gravitational waves detectors based on AIs and optical clocks have been proposed [16–23].

In this Letter, we demonstrate atom interferometry based on the ultranarrow $^1S_0$-$^3P_0$ optical clock transition of ^{88}Sr at $\lambda = 698$ nm both for a single AI (gravimeter) and for two simultaneous AIs in a differential scheme (gravity gradiometer). While atom interferometry based on intercombination transitions of calcium and magnesium has been reported already [24–27], the virtually infinite lifetime of the upper clock state in strontium is crucial for demanding applications. For example, as proposed in Refs. [18,19], the differential scheme demonstrated here might allow us to detect gravitational waves in the low-frequency range using a single-arm large-scale AI. This novel sensor will also enable new fundamental tests lying at the border of quantum mechanics and general relativity [28,29], such as the quantum interference of clocks, with the possible observation of the redshift induced decoherence effects [30,31], a light dark matter search [32], and tests of the weak equivalence principle with quantum superpositions of states with large energy (∼eV) separation [33]. Precision measurements of gravity will also be necessary for the development of optical lattice clocks. The comparisons of clocks at the 10^{-19} level will not only require a precise knowledge of the static gravitational field component at the atomic cloud location, but it will also demand a simultaneous measurement of time-varying gravitational potential effects down to the exceptional level of 10^{-2} m^2/s^2 [34]. Novel single-photon AIs, based on the same atomic transition employed as a frequency reference in optical lattice clocks, will then play an important role in this field by enabling advanced experimental sequences with interleaved precision measurements of the optical frequency and the gravitational potential.

In our experiment, a Mach-Zehnder-type AI is generated by the interaction of the freely falling Sr atoms with a $\pi/2$-π-$\pi/2$ sequence of laser pulses whose frequency ω is resonant with the optical atomic clock frequency ω_a (Fig. 1). The phase shift $\Delta\Phi$ between the two AI arms is given by [19,35]

$$\Delta\Phi = \left(\alpha - g\frac{\omega}{c}\right)T^2\left[1 + \left(2 + \frac{4}{\pi}\right)\frac{\tau}{T} + \frac{8}{\pi}\left(\frac{\tau}{T}\right)^2\right] + (\phi_1 - 2\phi_2 + \phi_3), \quad (1)$$

where τ is the duration of the $\pi/2$ pulse, T is the free-fall time between two subsequent pulses, α is the frequency chirping rate applied to the clock laser pulses to compensate for the gravity-induced Doppler shift, and $\phi_i = \omega z_i/c - \omega t_i$ are the phases of the clock laser field at positions z_i and times t_i at the beginning of each optical pulse.

The implementation of a single-photon AI poses several challenges. High-power and high-frequency-stability laser systems are required to drive the high-Q optical clock transition with a sufficiently high Rabi frequency. This condition is even more stringent in the case of large momentum transfer beam splitters [19,36]. As Eq. (1) shows, single-photon AIs are sensitive to the optical phase

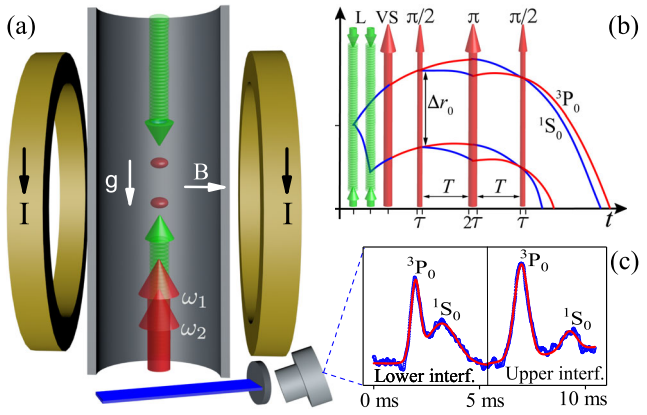

FIG. 1. (a) Simplified scheme of the apparatus in the double-cloud gradiometer configuration. Two cold ^{88}Sr clouds are launched vertically upwards using an accelerated optical lattice at 532 nm (green arrows). The velocity selection and the $\pi/2$-π-$\pi/2$ interferometric sequence are realized using laser pulses resonant with the clock transition (vertical red arrows). Two laser fields with frequencies ω_1 and ω_2 and linear parallel polarizations are used to simultaneously interrogate the two clouds. The clock transition is induced by a static magnetic field **B** parallel to the polarization of the laser fields. At the end of the interferometer sequence, a vertical push beam at 689 nm from the bottom side (not shown) is used to decelerate atoms in the ground state for spatially separating them from atoms in the excited state. After repumping the excited atoms back into the ground state, the relative population in the two output ports of each AI is detected by collecting onto a photomultiplier tube the fluorescence light produced by a resonant sheet of blue light at 461 nm. (b) Space-time trajectories of the atoms in the single-photon gradiometer. L, launch; VS, velocity selection. (c) Typical fluorescence signals at the output of the two AIs.

of the clock laser field, that is, to the phase difference of the laser field with respect to the atomic phase, rather than to the phase difference between two laser fields, as in multi-photon Raman or Bragg AIs. This sets stringent requirements on the phase stability of the laser employed to drive the clock transition. For instance, a small fluctuation in the optical path ~200 nm between the clock laser and the atoms induces a phase change larger than $\pi/2$ that is large enough to mask the AI signal. Therefore, to exploit the benefit of using the clock transition in atom interferometry, techniques to actively cancel the phase noise of the optical field or differential interferometric schemes need to be employed.

To drive the optical clock transition, we employed a 1 Hz–linewidth laser delivering up to 350 mW at $\lambda = 698$ nm. The system is based on a master laser frequency stabilized to a high finesse cavity [37]; it is power amplified by a slave laser and a tapered amplifier. For the double-cloud (gradiometer) experiments, the clock laser includes two frequency components ω_1 and ω_2 in order to simultaneously interact with both atomic samples. This is implemented by passing the clock laser beam in an acousto-optical modulator fed with two frequencies produced by a two-channel direct digital synthesizer generator. The AI pulses at different frequencies share the same optical path including fiber, mirrors, and optics, then acquiring only common-mode noise. With a $1/e^2$ beam radius of 500 μm, the typical peak intensity of each frequency on the atoms is about 10 W/cm^2.

The experiment was performed using the most abundant isotope of strontium, ^{88}Sr, for which the $J = 0 - J = 0$ optical clock transition is strictly forbidden but can be induced and tuned in its strength by a static magnetic field [38]. The procedure to produce ultracold samples of strontium has been described elsewhere [3,39]. In brief, a cloud of $\sim 5 \times 10^6$ ultracold ^{88}Sr atoms at a temperature of 1.2 μK, with a horizontal (vertical) dimension of 300 μm (70 μm) at full width at half maximum, is produced by a two-stage magneto-optical trap (MOT). After the MOT cloud preparation stage, about 50% of the atoms are loaded into a vertical 1D optical lattice at 532 nm. The atoms are maintained in the trap for a time of about 65 ms, which is necessary to invert the current direction in one of the MOT coils in order to produce a homogeneous magnetic field **B** (Fig. 1).

The procedure to launch the atoms into the fountain is different for the case of a single cloud and for the double cloud: In the first case, the atoms are released from the trap by switching off adiabatically the lattice beam and fall freely. For the two-cloud configuration, we extended the technique used in Ref. [39] to perform a double launch from a single source: about 10% of the atoms in the lattice are accelerated vertically upwards in 8 ms by ramping down the frequency of the top lattice beam at a rate of 100 kHz/ms, corresponding to an acceleration of $2.7g$; the remaining atoms are retrapped after a variable free-fall time and a second cloud is launched upwards with the same method in 6 ms. With a free-fall time of 1 ms, we produce two clouds with a similar number of atoms ($\sim 2.5 \times 10^5$), a separation $\Delta r_0 = 1.9$ mm (limited by geometric constraints of the apparatus), and a velocity difference $\Delta v_0 = 5.3\hbar\omega_a/mc$ along the vertical axis (where m is the mass of the ^{88}Sr atom) leading to a slight increase of 0.3 mm in the cloud distance during the subsequent AI stage.

The atoms launched in the fountain are velocity selected in the vertical direction with a π pulse resonant with the clock transition. The remaining atoms in the ground state are blown away using light resonant with the dipole-allowed $^1S_0$-$^1P_1$ transition at 461 nm. Typically, about 4% of the atoms are selected, thus producing samples of about 10^4 atoms with a narrow vertical momentum width of $\sim 0.04\hbar\omega_a/c$ (Fig. 2). This shows that an ultranarrow clock transition can provide a free-falling ensemble of atoms with a very well-defined velocity, enabling high AI contrast [40].

After the velocity selection, the AI $\pi/2$-π-$\pi/2$ laser pulse sequence resonant with the optical clock transition is applied to the atoms. In this way, atomic "internal"

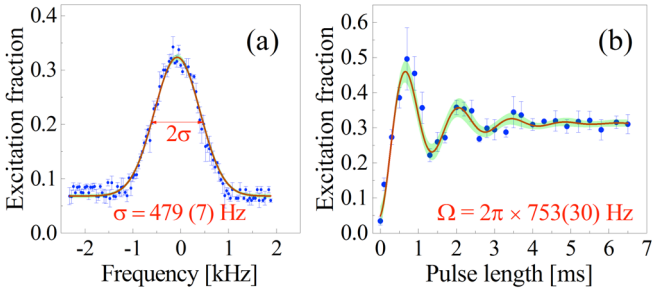

FIG. 2. (a) Clock spectroscopy signal on the free-falling, momentum selected cloud. The signal linewidth, by eliminating the effect of the finite spectroscopy pulse length (1.2 ms) and estimated from a Gaussian fit of the profile, indicates an atomic momentum spread of $0.04\hbar\omega_a/c$. (b) Rabi oscillations of the atomic excitation fraction as a function of the clock pulse length. The oscillation is recorded with typical values of the static magnetic field ($B = 330$ G) and clock light peak intensity (20 W/cm^2). The experimental result fits well with a damped sinusoid with a corresponding Rabi frequency of $\Omega = 2\pi \times 753(30)$ Hz and a damping time of 1.18(0.15) ms.

(electronic) clock states and "external" (momentum) states are entangled. At the end of the AI sequence, a push beam resonant with the intercombination $^1S_0$-$^3P_1$ transition at 689 nm propagating upwards is used to decelerate atoms in the ground state and spatially separate them from atoms in the excited state. After repumping the excited atoms back to the ground state, the relative population in the two AI outputs is detected by collecting the fluorescence signal produced by a resonant sheet of blue light at 461 nm onto a photomultiplier tube (Fig. 1).

The interference fringes obtained for the single AI (gravimeter) are shown in Fig. 3. We compared the observed fringe contrast and visibility with and without actively stabilizing the clock laser phase at the fiber end [41,42]. The main sources of phase noise are indeed acoustic and subacoustic vibrations coupled to the atomic system and to the 10 m–long polarization maintaining fiber used to bring the clock laser light to the atoms. The active fiber noise cancellation (FNC) system has a bandwidth of 50 kHz, reducing by more than 50 dB the phase noise up to 100 Hz [inset in Fig. 3(e)]. With this system, we observed a dramatic difference for the fringe visibility when the FNC is active (Fig. 3). This is particularly clear for the fringes corresponding to the longest AI time. The fringe visibility is only partially recovered by the FNC system, as shown in Fig. 3(d), because of uncompensated phase noise introduced by the optical components outside the loop before the atomic cloud.

The observed AI visibility and contrast are affected by the π-pulse efficiency ~50% [Fig. 2(b)] limited mainly by the initial atomic momentum width. The pulse duration for the momentum selection is indeed a trade-off between the number of selected atoms and the momentum width. A longer selection pulse would lead to an increase of the π pulse efficiency at the expense of the final atom number in the AI. The chosen parameters are the results of an optimization of the signal-to-noise ratio at the final detection. Further reduction of the contrast is due to clock laser intensity inhomogeneity (the clock beam size is comparable to the atomic cloud size) and to the residual motion of the atoms during the ~millisecond long π-pulse time. Using the fermionic ^{87}Sr isotope with the same laser intensity, the Rabi frequency would be $\Omega \sim 2\pi \times 5$ kHz, thus allowing a larger laser beam size or a shorter π-pulse duration. With a single-frequency clock laser peak intensity on the atomic

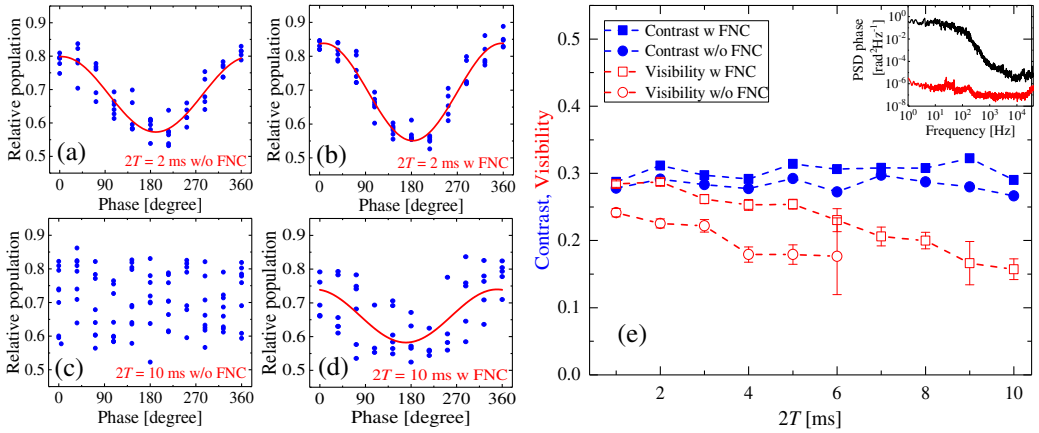

FIG. 3. Results for the single AI (gravimeter). AI fringes in (a) and (b) were observed for $2T = 2$ ms, with and without the active fiber noise cancellation (FNC) system, respectively; AI fringes in (c) and (d) correspond to $2T = 10$ ms, with and without FNC, respectively. (e) Measured contrast and fringe visibility as a function of $2T$. Fringe visibility (red open squares and circles) is given by the amplitude of the fitted sinusoidal function on each data set. Contrast (solid squares and circles) is estimated by data dispersion from the 2nd to the 98th percentile. Both contrast and visibility are measured with (squares) and without (circles) FNC. The inset shows the in-loop phase noise power spectral density of the 10 m–long optical fiber connecting the clock laser source to the AI, with (lower red curve) and without (upper black curve) FNC, respectively.

sample of about 20 W/cm^2 and a maximum static magnetic field $B = 330$ G, the observed Rabi frequency is $\Omega = 2\pi \times 753(30)$ Hz, corresponding to a π-pulse duration $\tau_\pi = 0.7$ ms [see Fig. 2(b)]. While this value is larger than the typical Raman or Bragg pulse duration, it is important to notice that in the case of single-photon clock interaction, the losses due to spontaneous emission are largely reduced. This represents a considerable advantage with respect to two-photon Raman or Bragg pulses, where the spontaneous emission constitutes a major limitation to AI contrast so that short pulses and large detunings from the single-photon transition are typically required.

Results obtained for the two simultaneous AIs (gravity gradiometer) are shown in Fig. 4. In order to study the common-mode phase noise rejection in the differential configuration, data have been acquired without FNC. For the gravity gradiometer, the differential phase shift is given by [43,44]

$$\Delta\phi \approx \frac{\omega}{c}(\Gamma T^2)\Delta r_0 + \frac{\omega}{c}(\Gamma T^2)\Delta v_0 T + \delta\phi \equiv \delta\phi_r + \delta\phi_v + \delta\phi, \quad (2)$$

where Γ is the gravity gradient. The first two leading phase shift terms are induced by the separation Δr_0 and the velocity difference Δv_0 between the two clouds, corresponding to $\delta\phi_r \sim 10^{-6}$ rad and $\delta\phi_v \sim 10^{-7}$ rad for $T = 5$ ms, that are too small to be measured with our current sensitivity. This would result in a closed ellipse pattern when plotting the interference fringe signals of one AI versus the other, thus preventing a fitting of the data. In order to analyze the data, a synthetic phase $\delta\phi$ was introduced by adding a relative phase shift between the two radio-frequency signals used to drive the acousto-optical modulator acting on the clock laser beam. In this case, the observed ellipse angle will be the sum of the synthetic phase $\delta\phi$ and the other phase contributions. Compared to other methods, in which a relative phase shift $\delta\phi$ is introduced via artificial external gradients [43,45], here no additional fields or changes of the pulse wave number are required.

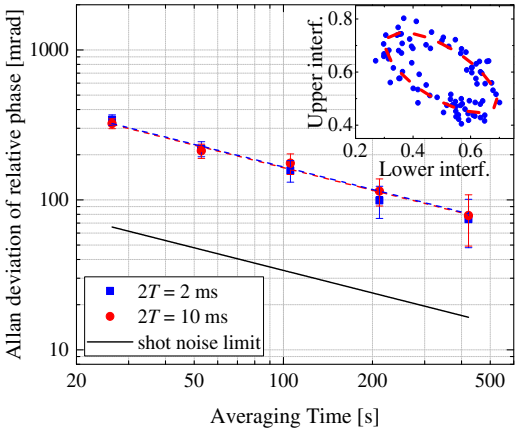

FIG. 4. Allan deviation of the relative phase shift for the gradiometer for two different AI durations. The gradiometer configuration rejects the common-mode phase noise with an Allan deviation scaling down as the square root of the averaging time, as shown by the fit to the data (dashed lines). The inset shows the output signal of the upper AI versus the signal of the lower AI for $2T = 10$ ms. The ellipse fitting (red dashed line) gives a relative phase $\Delta\phi = 2.31(0.06)$ rad that is consistent with the value of the applied synthetic phase $\delta\phi = 3\pi/4$ rad.

The effective suppression of common-mode phase noise in the gradiometer configuration is apparent when comparing the signals in Figs. 3 and 4; we estimate a suppression by at least 20 dB in the relevant frequency range. We characterized the gradiometer short-term sensitivity via the Allan deviation of the relative phase shifts for 1300 cycles for $2T = 2$ ms and $2T = 10$ ms (Fig. 4). The cycle time was set to 2.4 s, resulting in an overall acquisition time of about 1 h, for each set. Each ellipse was fit on 11 successive points. We find that the Allan deviation scales as the square root of the averaging time, showing that the residual noise is from white phase noise. The relative phase sensitivity at 400 s is approximately 82 mrad, which is 5 times higher than the shot-noise-limited sensitivity estimated for 10^4 atoms and with a typical contrast of ~30%. The current sensitivity is indeed limited by the photon collection efficiency at the output of the AI.

In conclusion, we have experimentally demonstrated a novel AI based on the ultranarrow clock transition of ^{88}Sr atoms. We implemented the scheme for a single AI (gravimeter) and for two simultaneous AIs (gravity gradiometer). We showed that the laser phase noise is drastically reduced in the gradiometric configuration, enabling the retrieval of the fringe visibility and contrast for an AI duration up to ~10 ms, limited by the present apparatus. The lattice double-launch technique and high frequency selectivity of the optical clock transition that we implemented allowed us to add a synthetic relative phase shift $\delta\phi$ with a novel method.

The new atom interferometry scheme we demonstrated will be important to investigate effects at the boundaries of quantum mechanics and general relativity. In the future, the implementation of this scheme in very-long-baseline gradiometers might allow us to detect gravitational waves in the so far unexplored low-frequency range. The clock transition in ^{87}Sr is also being considered for precision atom interferometry with atoms in optical waveguides [46].

We thank J. Ye for a critical reading of the Letter and G. Rosi and R. P. Del Aguila for useful discussions. We acknowledge financial support from INFN and the Italian Ministry of Education, University and Research (MIUR) under the Progetto Premiale "Interferometro Atomico" and PRIN 2015. This project has received funding from the Initial Training Network (ITN) supported

by the European Commission's 7th Framework Programme under Grant Agreement No. 607493. L. Hu acknowledges support by Kayser Italia.

*Also at ICTP, Trieste, Italy.
†Also at CNR-INO, Firenze, Italy.
poli@lens.unifi.it
‡Also at CNR-IFAC, Sesto Fiorentino, Italy.
guglielmo.tino@unifi.it

[1] *Proceedings of the International School of Physics "Enrico Fermi," Course CLXXXVIII*, Atom Interferometry, edited by G. M. Tino and M. A. Kasevich (SIF and IOS Press, Bologna, Amsterdam, 2014).
[2] T. Kovachy, P. Asenbaum, C. Overstreet, C. A. Donnelly, S. M. Dickerson, A. Sugarbaker, J. M. Hogan, and M. A. Kasevich, Nature (London) **528**, 530 (2015).
[3] N. Poli, F.-Y. Wang, M. G. Tarallo, A. Alberti, M. Prevedelli, and G. M. Tino, Phys. Rev. Lett. **106**, 038501 (2011).
[4] G. Rosi, F. Sorrentino, L. Cacciapuoti, M. Prevedelli, and G. M. Tino, Nature (London) **510**, 518 (2014).
[5] A. Peters, K. Y. Chung, and S. Chu, Nature (London) **400**, 849 (1999).
[6] R. Charriere, M. Cadoret, N. Zahzam, Y. Bidel, and A. Bresson, Phys. Rev. A **85**, 013639 (2012).
[7] Z.-K. Hu, B.-L. Sun, X.-C. Duan, M.-K. Zhou, L.-L. Chen, S. Zhan, Q.-Z. Zhang, and J. Luo, Phys. Rev. A **88**, 043610 (2013).
[8] J. M. McGuirk, G. T. Foster, J. B. Fixler, M. J. Snadden, and M. A. Kasevich, Phys. Rev. A **65**, 033608 (2002).
[9] F. Sorrentino, Q. Bodart, L. Cacciapuoti, Y.-H. Lien, M. Prevedelli, G. Rosi, L. Salvi, and G. M. Tino, Phys. Rev. A **89**, 023607 (2014).
[10] G. Rosi, L. Cacciapuoti, F. Sorrentino, M. Menchetti, M. Prevedelli, and G. M. Tino, Phys. Rev. Lett. **114**, 013001 (2015).
[11] P. Asenbaum, C. Overstreet, T. Kovachy, D. D. Brown, J. M. Hogan, and M. A. Kasevich, Phys. Rev. Lett. **118**, 183602 (2017).
[12] N. Poli, C. W. Oates, P. Gill, and G. M. Tino, Riv. Nuovo Cimento **36**, 555 (2013).
[13] A. D. Ludlow, M. M. Boyd, J. Ye, E. Peik, and P. O. Schmidt, Rev. Mod. Phys. **87**, 637 (2015).
[14] I. Ushijima, M. Takamoto, M. Das, T. Ohkubo, and H. Katori, Nat. Photonics **9**, 185 (2015).
[15] S. L. Campbell, R. B. Hutson, G. E. Marti, A. Goban, N. Darkwah Oppong, R. L. Mcnally, L. Sonderhouse, J. M. Robinson, W. Zhang, B. J. Bloom *et al.*, Science **358**, 90 (2017).
[16] G. M. Tino and F. Vetrano, Classical Quantum Gravity **24**, 2167 (2007).
[17] S. Dimopoulos, P. W. Graham, J. M. Hogan, M. A. Kasevich, and S. Rajendran, Phys. Rev. D **78**, 122002 (2008).
[18] N. Yu and M. Tinto, Gen. Relativ. Gravit. **43**, 1943 (2011).
[19] P. W. Graham, J. M. Hogan, M. A. Kasevich, and S. Rajendran, Phys. Rev. Lett. **110**, 171102 (2013).
[20] S. Kolkowitz, I. Pikovski, N. Langellier, M. D. Lukin, R. L. Walsworth, and J. Ye, Phys. Rev. D **94**, 124043 (2016).
[21] B. Canuel *et al.*, arXiv:1703.02490.
[22] M. A. Norcia, J. R. K. Cline, and J. K. Thompson, Phys. Rev. A **96**, 042118 (2017).
[23] L. Hollberg, E. H. Cornell, and A. Abdelrahmann, Phil. Trans. R. Soc. A **375**, 20160241 (2017).
[24] F. Riehle, T. Kisters, A. Witte, J. Helmcke, and C. J. Bordé, Phys. Rev. Lett. **67**, 177 (1991).
[25] U. Sterr, K. Sengstock, W. Ertmer, F. Riehle, and J. Helmcke, in *Atom Interferometry*, edited by P. Berman (Academic Press, New York, 1997), p. 293.
[26] F. Ruschewitz, J. L. Peng, H. Hinderthür, N. Schaffrath, K. Sengstock, and W. Ertmer, Phys. Rev. Lett. **80**, 3173 (1998).
[27] U. Sterr, C. Degenhardt, H. Stoehr, C. Lisdat, H. Schnatz, J. Helmcke, F. Riehle, G. Wilpers, C. Oates, and L. Hollberg, C.R. Phys. **5**, 845 (2004).
[28] Y. Margalit, Z. Zhou, S. Machluf, D. Rohrlich, Y. Japha, and R. Folman, Science **349**, 1205 (2015).
[29] G. Amelino-Camelia, Nat. Phys. **10**, 254 (2014).
[30] M. Zych, F. Costa, I. Pikovski, and Č. Brukner, Nat. Commun. **2**, 505 (2011).
[31] I. Pikovski, M. Zych, F. Costa, and Č. Brukner, Nat. Phys. **11**, 668 (2015).
[32] A. A. Geraci and A. Derevianko, Phys. Rev. Lett. **117**, 261301 (2016).
[33] G. Rosi, G. D'Amico, L. Cacciapuoti, F. Sorrentino, M. Prevedelli, M. Zych, Č. Brukner, and G. M. Tino, Nat. Commun. **8**, 15529 (2017).
[34] C. Voigt, H. Denker, and L. Timmen, Metrologia **53**, 1365 (2016).
[35] C. Antoine, Appl. Phys. B **84**, 585 (2006).
[36] R. H. Parker, C. Yu, B. Estey, W. Zhong, E. Huang, and H. Müller, Phys. Rev. A **94**, 053618 (2016).
[37] M. G. Tarallo, N. Poli, M. Schioppo, D. V. Sutyrin, and G. M. Tino, Appl. Phys. B **103**, 17 (2011).
[38] A. V. Taichenachev, V. I. Yudin, C. W. Oates, C. W. Hoyt, Z. W. Barber, and L. Hollberg, Phys. Rev. Lett. **96**, 083001 (2006).
[39] X. Zhang, R. P. del Aguila, T. Mazzoni, N. Poli, and G. M. Tino, Phys. Rev. A **94**, 043608 (2016).
[40] S. S. Szigeti, J. E. Debs, J. J. Hope, N. P. Robins, and J. D. Close, New J. Phys. **14**, 023009 (2012).
[41] L.-S. Ma, P. Jungner, J. Ye, and J. L. Hall, Opt. Lett. **19**, 1777 (1994).
[42] F. Riehle, Nat. Photonics **11**, 25 (2017).
[43] A. Roura, Phys. Rev. Lett. **118**, 160401 (2017).
[44] Equation (2) does not include the correction for the finite pulse duration, the change of the cloud separation during the interferometer time, and the small difference between the two laser frequencies ω_1 and ω_2.
[45] Y.-P. Wang, J.-Q. Zhong, X. Chen, R.-B. Li, D.-W. Li, L. Zhu, H.-W. Song, J. Wang, and M.-S. Zhan, Opt. Commun. **375**, 34 (2016).
[46] T. Akatsuka, T. Takahashi, and H. Katori, Appl. Phys. Express **10**, 112501 (2017).